Am J Transl Res 2026;18(3):1910-1922
www.ajtr.org /ISSN:1943-8141/AJTR0171284

Original Article

A multiparametric magnetic resonance imaging model incorporating the relative apparent diffusion coefficient for preoperative discrimination of triple-negative breast cancer

Haiyun Fan[1*], Wanyi Shao[1*], Xin Zhou[2], Yuxuan Chen[2], Yuanqing Liu[1], Hao Zhou[3], Juanmin Zha[4], Jian Wang[5], Xinxing Ma[1], Yue Teng[1]

[1]Department of Radiology, The First Affiliated Hospital of Soochow University, Suzhou 215006, Jiangsu, China; [2]Department of Medical Imaging Science, Suzhou Medical College of Soochow University, Suzhou 215006, Jiangsu, China; [3]Department of General Surgery, The First Affiliated Hospital of Soochow University, Suzhou 215006, Jiangsu, China; [4]Department of Oncology, The First Affiliated Hospital of Soochow University, Suzhou 215006, Jiangsu, China; [5]Department of Gastroenterology, Changzheng Hospital of Naval Medical University, Shanghai 200003, China. [*]Equal contributors.

Received January 6, 2026; Accepted March 4, 2026; Epub March 15, 2026; Published March 30, 2026

Abstract: Objectives: To explore the value of a multiparametric MRI combined model based on morphology, hemodynamics, and apparent diffusion coefficient (ADC) in differentiating triple-negative breast cancer (TNBC) from non-triple-negative breast cancer (non-TNBC). Methods: A retrospective study was conducted on 213 breast cancer patients (64 TNBC, 149 non-TNBC). Morphological, hemodynamic, mean apparent diffusion coefficient (ADC), and relative apparent diffusion coefficient (rADC) features were compared. Feature selection was performed using LASSO, and a multiparametric combined model was constructed using logistic regression. Diagnostic performance was evaluated using receiver operating characteristic (ROC) curves and DeLong tests. Calibration and clinical utility were evaluated using the Hosmer-Lemeshow test, calibration curves, and decision curve analysis (DCA). Results: TNBC tended to present as unifocal lesions with hyperintensity on T2WI. They also frequently showed cystic necrosis, peritumoral edema, and Type II/III curve patterns (all $P < 0.05$). The diagnostic performance of rADC1 (AUC = 0.669) was better than that of mean ADC and rADC2. Multifocality/multicentricity, peritumoral edema, and rADC1 were independent predictors of TNBC. The combined model achieved an AUC of 0.772, 67.19% sensitivity, 77.18% specificity, and 84.6% negative predictive value, performing better than single-parameter models (all $P < 0.01$). The model showed good calibration and high clinical utility in DCA. Conclusions: The combined model - constructed based on multifocality/multicentricity, peritumoral edema, and the rADC1 value - can effectively predict TNBC preoperatively, has good discrimination, calibration, and clinical utility, and provides an important imaging reference basis for accurately identifying TNBC and formulating individualized diagnosis and treatment plans.

Keywords: Triple-negative breast cancer, magnetic resonance imaging, relative apparent diffusion coefficient, multiparametric MRI

Introduction

Breast cancer has currently become the most common malignant tumor in women worldwide, accounting for about 25% of female cancers, and its incidence rate is increasing annually [1]. Triple-negative breast cancer (TNBC) is a special type of breast cancer; due to the lack of estrogen receptor (ER), progesterone receptor (PR), and human epidermal growth factor receptor 2 (HER2), it often has a relatively high histological grade and is prone to lung metastasis, brain metastasis, etc. [2, 3]. TNBC lacks endocrine or anti-HER2 targets, and currently relies mainly on neoadjuvant chemotherapy. Breast cancer is a highly heterogeneous tumor. Preoperative needle biopsy is the gold standard for identifying TNBC, but due to sampling errors,

https://doi.org/10.62347/SGZO1989

it cannot reflect the heterogeneity of the entire breast tumor. Therefore, preoperative non-invasive identification of TNBC is crucial for patients' individualized treatment choices [4].

Multiparametric magnetic resonance imaging (MRI), by integrating morphological, hemodynamic, and diffusion characteristics, has unique advantages in the differential diagnosis of breast tumors. Among them, diffusion-weighted imaging (DWI) uses the apparent diffusion coefficient (ADC) value to quantitatively reflect the degree of water molecule diffusion inside and outside cells, thereby indirectly reflecting the degree of malignancy of breast tumors, and it has been widely used in the grading, differentiation, and prognosis evaluation of breast tumors [5]. Currently, the utility of ADC values in differentiating TNBC from other molecular subtypes remains controversial; Chen et al. believe that the ADC value of TNBC is lower than that of other types of breast cancer, but the study by Ohashi et al. found that there is no statistical difference in ADC values between TNBC and non-TNBC [6, 7]. The absolute ADC value is related to region of interest (ROI) delineation, magnetic field strength, *b*-value selection, scanning parameters, and individual differences [8-10]. The instability of the absolute ADC value limits its application in clinical practice [11, 12].

To solve the problem of the instability of absolute ADC values, we calculated the relative apparent diffusion coefficient (rADC) values. This reduced the inter-individual differences in absolute ADC values [13-15]. The rADC value is the ratio of the lesion ADC value to the ADC value of a reference tissue (such as the pectoralis major muscle or normal gland). This improves the accuracy of differential diagnosis [13, 14]. Currently, the rADC value has been applied in the differentiation of benign and malignant breast tumors. rADC value, however, has not yet been fully explored in differentiating TNBC from non-TNBC [16].

This study aims to construct a differential diagnostic model for TNBC and non-TNBC. We combined multiparametric MRI features, such as morphology, hemodynamics, mean ADC values, and rADC values. This aims to improve the diagnostic accuracy of TNBC, reduce unnecessary biopsies, and guide clinicians in performing individualized treatment.

Materials and methods

Study population

This study was approved by the Ethics Committee of the First Affiliated Hospital of Soochow University, and informed consent from subjects was waived (approval number: [2025] 1276). We retrospectively analyzed 302 pathologically confirmed breast cancer patients from the First Affiliated Hospital of Soochow University from February 2016 to February 2023. They had not received any treatment before the MRI examination.

The exclusion criteria were as follows: (1) pregnancy or lactation (n = 15); (2) lesions presenting as nonmass enhancement (NME; n = 57); (3) severe image artifacts, incomplete or missing data (n = 17). A total of 89 patients were excluded for the above reasons. Ultimately, 213 patients were included in this study.

Immunohistochemical analysis was performed according to the American Society of Clinical Oncology/College of American Pathologists guidelines [17, 18]. These included 64 TNBC patients and 149 non-TNBC patients. Detailed exclusion criteria are shown in **Figure 1**.

MRI acquisition

Images were acquired on a 3.0-T system (MAGNETOM Skyra, Siemens Healthineers, Germany). A dedicated breast phased-array coil was used. Patients lay supine and feet-first within the scanner. Both breasts were naturally suspended and held in place. The imaging protocol included standard non-contrast sequences, DWI, and dynamic contrast-enhanced (DCE) MRI.

Acquisition parameters are described below:

Routine noncontrast sequences: Axial 3D FLASH T1WI: TR/TE, 6/2.5 ms; flip angle, 10°; slice thickness, 1.2 mm; FOV, 340 × 340 mm; matrix, 320 × 320.

Axial fat-suppressed T2WI: TR/TE, 4490/53 ms; inversion time, 230 ms; slice thickness, 4 mm; matrix, 320 × 320.

DWI: An axial single-shot echo-planar imaging sequence with fat suppression was used with

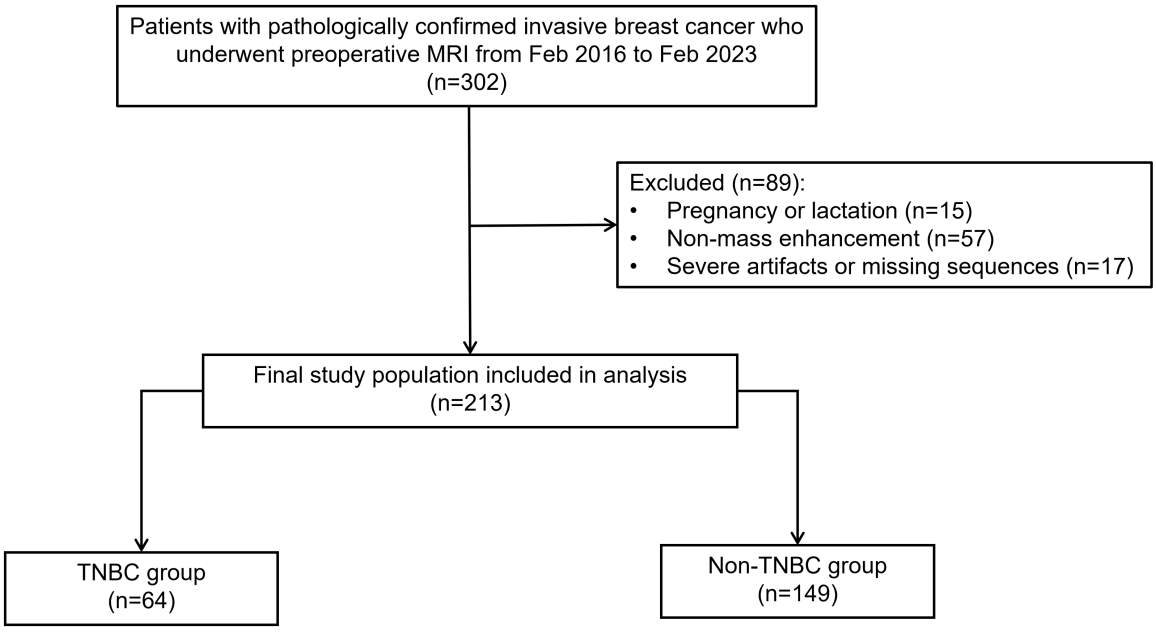

Figure 1. Flowchart of the patient selection process. TNBC, triple-negative breast cancer; NME, non-mass enhancement; MRI, magnetic resonance imaging.

the following parameters: TR, 10,400 ms; TE, 53 ms; *b*-values, 0 and 800 s/mm^2 [11]; slice thickness, 4 mm; number of excitations (NEX), 4; matrix, 128 × 128.

DCE-MRI: A 3D volumetric interpolated breath-hold examination sequence was initiated with a pre-contrast mask scan, including the following parameters: TR, 4.5 ms; TE, 1.7 ms; flip angle, 15°; slice thickness, 1.2 mm (no gap); temporal resolution, 58 s/phase. Gd-DTPA (Bayer Healthcare, Germany) was administered intravenously through the antecubital vein at a bolus dose of 0.1 mmol/kg and a flow rate of 3.0 mL/s, followed immediately by a 20-mL saline flush at the same rate. Five consecutive postcontrast dynamic phases were acquired.

Image analysis and data collection

(1) Image review and quality control: Two radiologists independently reviewed the MRI scans. Both experts had over 10 years of experience in breast imaging and were blinded to clinical and pathologic results during assessment. All measurements were performed on a Neusoft PACS workstation (Neusoft Medical Systems, Shenyang, China). For qualitative features, disagreements were resolved by consensus. For quantitative data, the mean of both measurements was calculated to reduce interobserver variability. Clinical variables, including age, pathologic type, and immunohistochemical markers, were extracted directly from electronic medical records.

(2) Morphological and hemodynamic feature analysis: MRI features were assessed following the ACR BI-RADS lexicon. Morphological analysis covered multifocal/multicentric status, shape, margins, T2WI signal intensity, necrosis, and peritumoral edema. Hemodynamic analysis included internal enhancement patterns, early enhancement rate (EER) tiers (slow < 50%; medium 50%-100%; rapid > 100%), and time-intensity curves (TIC; Type I: persistent > 10%; Type II: plateau ± 10%; Type III: washout > 10%).

(3) Quantitative analysis of diffusion-weighted imaging (ADC and rADC): Qualitative lesion signal on DWI (b = 800 s/mm^2) was first graded using a four-point scale (hypointense, isointense, slightly hyperintense, and hyperintense). For quantitative analysis, the second DCE phase guided ROI placement (4-25 mm^2) within the most avidly enhancing solid component while avoiding necrosis and vessels. Three measurements were averaged to improve stability. Relative ADC indices were then calculat-

Table 1. Baseline clinicopathological characteristics of the study population

Characteristics	TNBC (n = 64) No. (%)	Non-TNBC (n = 149) No. (%)	χ^2/t Value	*P* Value
Age (years)			-0.416	0.677
Median [IQR]	44.5 [38.0, 56.0]	46 [37.0, 53.0]		
Menopausal Status			2.334	0.127
Premenopausal	43 (67.2)	115 (77.2)		
Postmenopausal	21 (32.8)	34 (22.8)		
Histological Type			2.177	0.337
IDC	57 (89.1)	124 (83.2)		
ILC	2 (3.1)	13 (8.7)		
Others	5 (7.8)	12 (8.1)		
Histological Grade			44.294	< 0.001
Grade I	0 (0)	17 (11.4)		
Grade II	12 (18.8)	84 (56.4)		
Grade III	52 (81.3)	48 (32.2)		
Tumor Size (cm)				
Mean ± SD	2.88 ± 2.21	2.47 ± 1.85	-1.916	0.055

IDC, invasive ductal carcinoma; ILC, invasive lobular carcinoma; IQR, interquartile range; SD, standard deviation; TNBC, triple-negative breast cancer.

ed using internal references: rADC1 was defined as the ratio of mean lesion ADC to mean ipsilateral pectoralis major muscle ADC, whereas rADC2 was calculated as mean lesion ADC divided by mean contralateral normal gland ADC.

Statistical analysis

Statistical analyses were performed using SPSS (v24.0; IBM Corp., NY, USA) and R (v4.0.4; The R Foundation for Statistical Computing, Vienna, Austria). The Kolmogorov-Smirnov test was used to test the normality of continuous variables. Normally distributed data are presented as mean ± standard deviation. Comparisons between groups were performed using the independent samples *t* test. Non-normally distributed data are expressed as median (interquartile range [IQR]). They were analyzed using the Mann-Whitney *U* test. Categorical variables are presented as frequencies and percentages. They were compared using the χ^2 test or Fisher's exact test.

Feature selection was performed through univariate analysis. Factors with $P < 0.05$ were retained. Collinearity analysis was performed through a Pearson correlation matrix. A model for predicting TNBC was constructed through multivariate logistic regression. Odds ratios (ORs) and 95% confidence intervals (CIs) were calculated.

Internal validation was performed through 100 leave-group-out cross-validations.

Diagnostic performance was evaluated through sensitivity and specificity. Our sample size was moderate. Therefore, more stable and reliable area under the curve (AUC) estimates and their CIs were obtained through Bootstrap resampling. The DeLong test was used to compare the AUC values of different models. The Hosmer-Lemeshow test and calibration curves were used to evaluate the consistency of the model. The clinical net benefit of the model was evaluated through decision curve analysis (DCA). All tests were two-sided, and a P value < 0.05 was considered statistically significant.

Results

Baseline characteristics of the TNBC and non-TNBC groups

A total of 213 breast cancer patients were enrolled in this study. Among them, 64 had TNBC and 149 had non-TNBC. No statistically significant differences were found between the two groups in age, menstrual status, histological type, and tumor size ($P > 0.05$). There was a statistical difference in histological grade between the two groups. The TNBC group had a

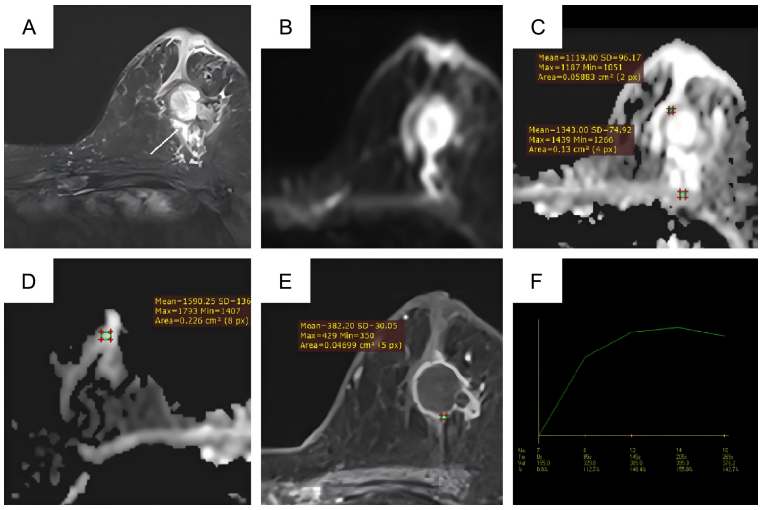

Figure 2. Representative images of a 55-year-old woman with triple-negative breast cancer (TNBC). A. Axial fat-suppressed T2-weighted image reveals an irregular mass with hyperintensity (suggesting cystic necrosis) and peritumoral edema (white arrow). B. Diffusion-weighted imaging (DWI) demonstrates high signal intensity. C. On the apparent diffusion coefficient (ADC) map, the mean ADC value of the lesion is 1.119 × 10^{-3} mm^2/s, and the rADC1 (lesion/pectoralis major muscle) is 0.83. D. On the ADC map, the rADC2 (lesion/contralateral normal gland) is 0.70. E. Early-phase dynamic contrast-enhanced MRI (DCE-MRI) depicts distinct rim enhancement. F. The time-intensity curve (TIC) exhibits a plateau pattern (Type II).

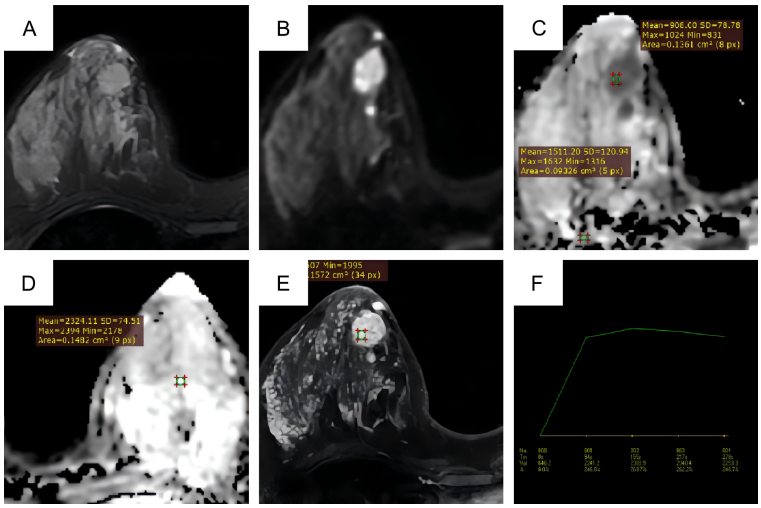

Figure 3. Representative images of a 26-year-old woman with non-TNBC (Luminal B subtype). A. Axial fat-suppressed T2-weighted image reveals an oval-shaped mass with isointensity, demonstrating the absence of cystic necrosis and peritumoral edema. B. Diffusion-weighted imaging (DWI) demonstrates high signal intensity. C. On the ADC map, the mean ADC value is 0.908 × 10^{-3} mm^2/s, and the rADC1 (lesion/pectoralis major muscle) is 0.50. D. On the ADC map, the rADC2 (lesion/contralateral normal gland) is 0.39. E. Early-phase DCE-MRI exhibits heterogeneous enhancement. F. The time-intensity curve (TIC) shows a plateau pattern (Type II).

higher histological grade, with 81.3% being Grade III (P < 0.001). **Table 1** lists the baseline clinicopathologic characteristics of all patients.

MRI morphological manifestations

Differences in lesion distribution (P = 0.014), T2WI Signal Intensity (P = 0.007), cystic necrosis (P < 0.001), and peritumoral edema (P < 0.001) between the two groups were statistically significant. Differences in shape (P = 0.691) and margin (P = 0.600) were not statistically significant. The TNBC group was more prone to being unifocal than the non-TNBC group. T2WI Signal Intensity often showed hyperintensity. The lesions were often accompanied by cystic necrosis and peritumoral edema. **Figure 2** shows a TNBC case with typical features. Non-TNBC lesions often showed isointensity or hyperintensity on T2WI and lacked peritumoral edema (**Figure 3**). **Table 2** lists the morphological features of the two groups of cases.

Hemodynamic characteristics of DCE-MRI

The difference in internal enhancement characteristics of lesions between the two groups was statistically significant (P < 0.001). The difference in TIC patterns was statistically significant (P = 0.001). There was no significant statistical difference in EER between the two groups (P = 0.997). The TNBC group mainly showed rim enhancement. The TIC patterns were mainly plateau (Type II) or washout (Type III) patterns (**Table 2**).

DWI signal profiling and quantitative ADC/rADC metrics

The difference in DWI signal intensity distribution of lesions between the two groups was statistically significant (P = 0.033; **Table 2**). Both groups mainly showed hyperintensity. The mean ADC, rADC1,

Table 2. Comparison of MRI features between TNBC and non-TNBC groups

Characteristics	TNBC (n = 64) No. (%)	Non-TNBC (n = 149) No. (%)	χ^2/Z Value	*P* Value
Multifocal/multicentric			6.183	0.014
No (Unifocal)	58 (90.6)	113 (75.8)		
Yes	6 (9.4)	36 (24.2)		
Shape			0.223	0.691
Oval	12 (18.8)	24 (16.1)		
Round	0 (0.0)	0 (0.0)		
Irregular	52 (81.3)	125 (83.9)		
Margin			0.458	0.600
Circumscribed	7 (10.9)	12 (8.1)		
Not circumscribed	57 (89.1)	137 (91.9)		
T2WI Signal Intensity			10.046	0.007
Hypointense	1 (1.6)	7 (4.7)		
Isointense	6 (9.4)	40 (26.8)		
Hyperintense	57 (89.1)	102 (68.5)		
DWI Signal Intensity			6.824	0.033
Hypointense	0 (0.0)	0 (0.0)		
Isointense	2 (3.1)	0 (0.0)		
Slightly hyperintense	8 (12.5)	10 (6.7)		
Hyperintense	54 (84.4)	139 (93.3)		
Cystic Necrosis			15.664	< 0.001
Absent	37 (57.8)	124 (83.2)		
Present	27 (42.2)	25 (16.8)		
Peritumoral Edema			18.600	< 0.001
Absent	27 (42.2)	109 (73.2)		
Present	37 (57.8)	40 (26.8)		
Internal Enhancement Characteristics			57.547	< 0.001
Homogeneous	1 (1.6)	9 (6.0)		
Heterogeneous	28 (43.8)	128 (85.9)		
Rim enhancement	33 (51.6)	12 (8.1)		
Dark internal septations	2 (3.1)	0 (0.0)		
Early Enhancement Rate (EER)			-	0.997
Rapid	61 (95.3)	142 (95.3)		
Medium	3 (4.7)	7 (4.7)		
Slow	0 (0.0)	0 (0.0)		
Time-Intensity Curve (TIC) Pattern			13.175	0.001
Persistent (Type I)	5 (7.8)	9 (6.0)		
Plateau (Type II)	33 (51.6)	113 (75.8)		
Washout (Type III)	26 (40.6)	27 (18.1)		

DWI, diffusion-weighted imaging; EER, early enhancement rate; T2WI, T2-weighted imaging; TIC, time-intensity curve; TNBC, triple-negative breast cancer. $P < 0.05$ indicates a statistically significant difference. Dashes (-) indicate that the value is not applicable (Fisher's exact test was used).

and rADC2 values in the TNBC group were higher than those in the non-TNBC group ($P = 0.001$, $P < 0.001$, and $P = 0.042$, respectively; **Table 3**). Receiver operating characteristic (ROC) analysis showed that the AUC of rADC1 was 0.669. DeLong test results showed that the diagnostic performance of rADC1 was significantly better than that of the mean ADC (AUC = 0.646; $P = 0.002$). The diagnostic performance of rADC1 was also significantly better than that of rADC2 (AUC = 0.627; $P = 0.004$) (**Table 4** and **Figure 4**).

Table 3. Quantitative comparison of ADC and relative ADC (rADC) metrics between TNBC and non-TNBC groups

Parameters	TNBC (n = 64)	non-TNBC (n = 149)	*t* Value	*P* Value
ADC Values (10^{-3} mm^2/s)				
Lesion	1.02 ± 0.15	0.95 ± 0.16	3.374	0.001
Ipsilateral Pectoralis Major	1.60 ± 0.2	1.66 ± 0.2	-2.156	0.032
Contralateral Normal Gland	1.89 ± 0.33	1.94 ± 0.38	-0.862	0.390
Relative ADC Indices				
rADC1 (Lesion/Muscle)	0.66 ± 0.14	0.58 ± 0.11	4.556	< 0.001
rADC2 (Lesion/Gland)	0.55 ± 0.12	0.51 ± 0.16	2.044	0.042

ADC, apparent diffusion coefficient; rADC, relative apparent diffusion coefficient; SD, standard deviation; TNBC, triple-negative breast cancer. Data are presented as mean ± SD. Statistical comparisons were performed using the independent samples t-test. rADC1 = mean lesion ADC/mean ipsilateral pectoralis major muscle ADC; rADC2 = mean lesion ADC/mean contralateral normal gland ADC.

Table 4. Diagnostic performance of ADC, relative ADC indices, and the combined model in differentiating TNBC

Parameters	AUC (95% CI)	Cut-off Value	Sensitivity (%) (95% CI)	Specificity (%) (95% CI)	PPV (%)	NPV (%)	*P* Value***
Lesion Mean ADC	0.646 (0.561-0.724)	0.348	45.31 (0.328-0.583)	79.19 (0.718-0.854)	48.3	77.1	0.002
rADC1	0.669 (0.589-0.743)	0.296	64.06 (0.511-0.757)	65.10 (0.569-0.727)	44.1	80.8	0.004
rADC2	0.627 (0.532-0.699)	0.266	84.38 (0.731-0.922)	37.58 (0.298-0.459)	36.7	84.8	0.004
Combined Model	0.772 (0.701-0.841)	0.322**	67.19 (0.543-0.784)	77.18 (0.696-0.837)	55.8	84.6	Reference

ADC, apparent diffusion coefficient; AUC, area under the receiver operating characteristic curve; CI, confidence interval; rADC, relative apparent diffusion coefficient; TNBC, triple-negative breast cancer. rADC1 = mean lesion ADC/mean ipsilateral pectoralis major muscle ADC; rADC2 = mean lesion ADC/mean contralateral normal gland ADC. **For the combined model, the cut-off value represents the predicted probability threshold. ***P values were calculated using the DeLong test to compare the AUC of each single parameter against the combined model.

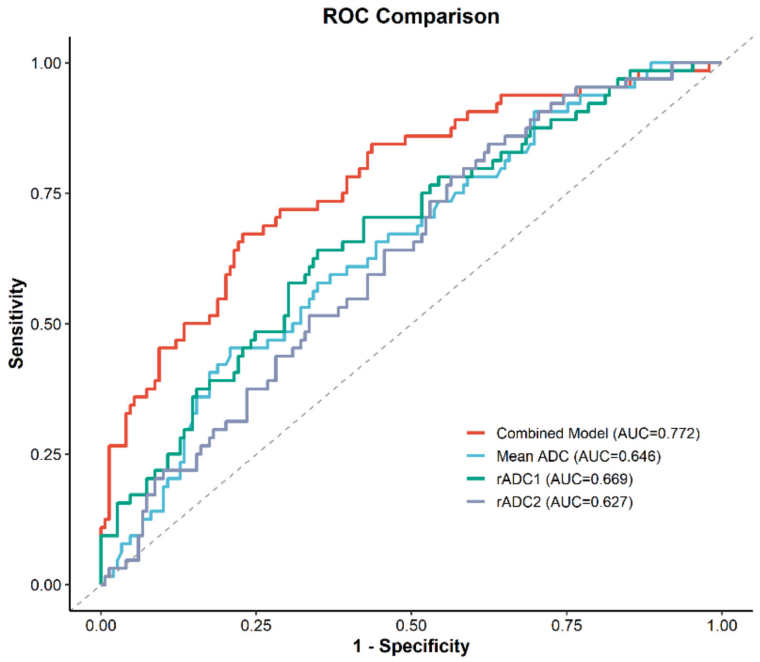

Figure 4. Comparison of diagnostic efficacy using receiver operating characteristic (ROC) curves. ADC, apparent diffusion coefficient; AUC, area under the curve; rADC, relative apparent diffusion coefficient; TNBC, triple-negative breast cancer.

Construction and evaluation of the combined model

Variables with $P < 0.05$ in the univariate analysis were entered into the LASSO regression model. This model was used to reduce dimensionality and select features (**Figure 5**). Four predictors were found based on the optimal λ. These predictors were rADC1, peritumoral edema, multifocality/multicentricity, and cystic necrosis. Then, the four predictors were included in a multivariate logistic regression analysis. rADC1 (OR = 209.784; $P < 0.001$), peritumoral edema (OR = 2.819; $P = 0.006$), and multifocality/multicentricity (OR = 0.279; $P = 0.012$) were independent predictors for TNBC. These findings are detailed in **Table 5**.

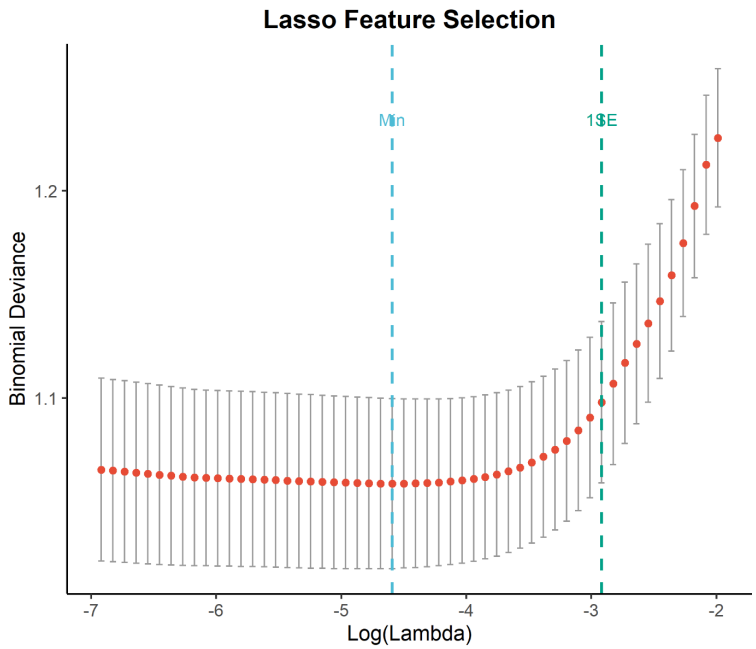

Figure 5. Feature selection using the least absolute shrinkage and selection operator (LASSO) binary logistic regression model. LASSO, least absolute shrinkage and selection operator.

The formula of the combined diagnostic model is as follows: *Logit(P)* = -4.553 + 5.346 × rADC1 + 1.036 × Edema - 1.277 × Multifocality. Variables were coded as binary: peritumoral edema, present = 1, absent = 0; multifocality, yes = 1, no = 0.

The AUC of the combined model reached 0.772 (95% CI: 0.702-0.842). The sensitivity and specificity were 67.19% (95% CI: 0.543-0.784) and 77.18% (95% CI: 0.696-0.837), respectively. The positive predictive value (PPV) and negative predictive value (NPV) of the combined model were 55.8% and 84.6%. The NPV of the single rADC2 model achieved 84.8%; however, its PPV was only 36.7%. The above results indicate that the combined model is more effective in identifying TNBC and can exclude non-TNBC. DeLong test results showed that the combined model had the highest AUC. It was superior to other single models (all $P < 0.01$; **Table 4** and **Figure 4**). The Hosmer-Lemeshow test and calibration curve showed that the predictive curve of the combined model overlapped well with the actual situation. This indicated that the combined model had the best calibration performance (**Figure 6**). The DCA curve results showed that the combined model had higher clinical utility than the single models. This was observed across a wide range of threshold probabilities (**Figure 7**).

Discussion

Based on the characteristics of MRI morphology, hemodynamics, and rADC, this study systematically compared the imaging differences between TNBC and non-TNBC, and constructed and evaluated the application value of a multiparametric MRI combined model in predicting TNBC. The results showed that the combined imaging model constructed using multifocality, peritumoral edema, and rADC1 values was significantly superior to traditional single imaging indicators in predicting TNBC. The combined model performed satisfactorily in the three dimensions of discrimination, calibration, and clinical utility. This study proposed for the first time using the rADC value as a key quantitative indicator for the differential diagnosis of TNBC, effectively overcoming the variability of individual ADC values and significantly improving the stability and reliability of the diagnosis [5, 11, 12]. It successfully constructed a multi-modal combined diagnostic model using morphological features and ADC parameters for the first time, breaking through the limitations of traditional reliance on single sequences or subjective morphological assessment, and providing a new strategy for the precise non-invasive diagnosis of TNBC. The application of this model contributes to the non-invasive early identification of TNBC and provides key imaging evidence for personalized treatment decisions for TNBC [2, 4].

Due to the lack of ER, PR, and HER2 expression, TNBC is more clinically aggressive [19]. Consistent with the findings of Rugengamanzi et al., our results showed that TNBC has a higher histological grade than non-TNBC [20]. MRI manifestations also reflect this pathological characteristic. The TNBC group often shows hyperintensity on T2WI, and lesions are often accompanied by cystic necrosis and peritumoral edema. These imaging features may be relat-

Table 5. Multivariate logistic regression analysis identifying independent predictors of TNBC

Variables	*β* Coefficients	S.E.	*P Value*	OR	95% *CI*
rADC1	5.346	1.437	< 0.001	209.784	(12.547-3507.649)
Peritumoral edema	1.036	0.375	0.006	2.819	(1.351-5.882)
Multifocal/multicentric	-1.277	0.510	0.012	0.279	(0.103-0.757)

β, regression coefficient; CI, confidence interval; OR, odds ratio; rADC, relative apparent diffusion coefficient; S.E., standard error; TNBC, triple-negative breast cancer. rADC1 = mean lesion ADC/mean ipsilateral pectoralis major muscle ADC.

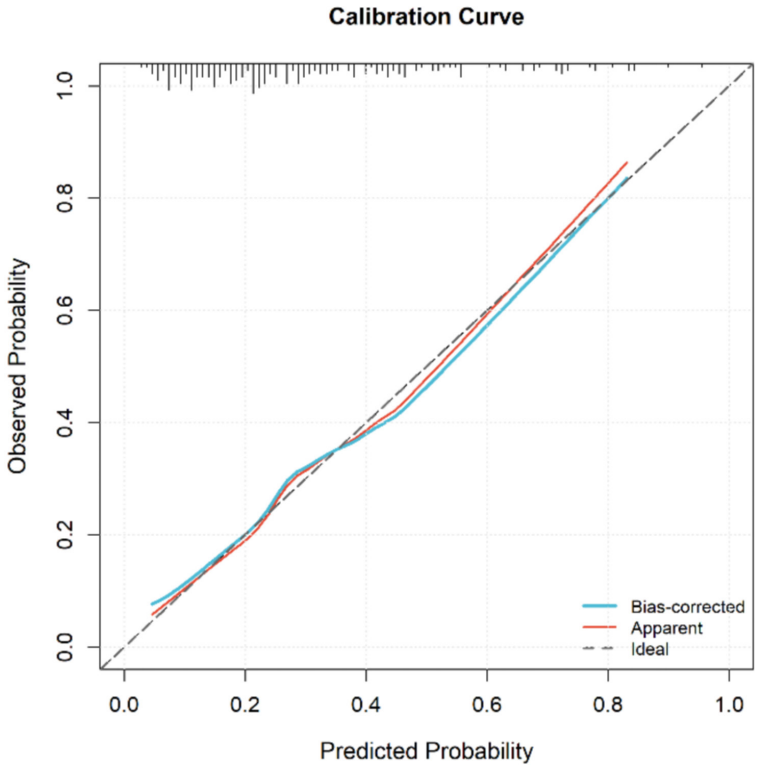

Figure 6. Calibration curve of the combined diagnostic model. TNBC, triple-negative breast cancer.

ed to the high aggressiveness of the tumor. TNBC grows rapidly, has high cell density, and has a higher Ki-67 level [21].

When the tumor growth rate exceeds the rate of neovascularization, it causes tumor ischemia and hypoxia, leading to necrosis. After necrosis, the effect of increased water content within the tumor outweighs the cellular effect, which increases the T2WI signal of the tumor [22]. In contrast, the non-TNBC group, especially luminal breast cancer, usually contains an abundant collagen stroma, and the incidence of tumor necrosis is lower than that in TNBC [23, 24].

Multivariate analysis showed that multifocality/multicentricity was a negative independent predictor (OR = 0.279). TNBC usually presents as a solitary lesion, and non-TNBC has a higher probability of multifocality. This difference in distribution patterns may be related to tumor growth patterns. TNBC usually grows by pushing the margins, while non-TNBC usually segments along the ducts, presenting a "jumping" growth pattern [25]. Peritumoral edema is an independent predictor of TNBC. This may be related to two mechanisms: elevated expression of vascular endothelial growth factor (VEGF) increases vascular permeability, while tumor emboli obstruct lymphatic vessels, causing impaired drainage [26]. Therefore, peritumoral edema is a valuable imaging marker for evaluating tumor aggressiveness.

DCE-MRI provides an important basis for differentiating TNBC from non-TNBC by evaluating tumor microvascular characteristics. This study found that the TIC curves of TNBC lesions often present as plateau (type II) or washout (type III) curves and often show rim enhancement [27]. This may be related to the aggressiveness of neovascularization, such as high intratumoral microvessel density, immature blood vessels, incomplete basement membranes, and large endothelial gaps [25]. The early rapid enhancement of TNBC stems from high vascular permeability and loose endothelial junctions, which promote the rapid extravasation of contrast agents into the extracellular space, followed by rapid clearance. Coupled with frequent cystic necrosis inside the tumor, a characteristic rim enhancement pattern is formed. In contrast,

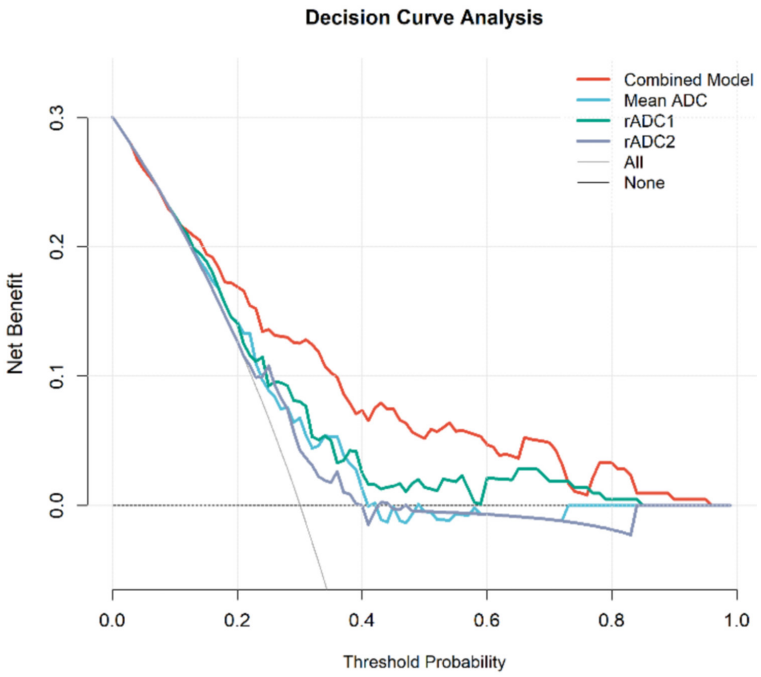

Figure 7. Evaluation of clinical utility via decision curve analysis (DCA). ADC, apparent diffusion coefficient; DCA, decision curve analysis; rADC, relative apparent diffusion coefficient; TNBC, triple-negative breast cancer.

non-TNBC lesions usually present as heterogeneous [28].

DWI provides an important basis for the differential diagnosis of breast tumors by detecting the degree of restricted Brownian motion of water molecules and providing the quantitative parameter ADC value [29]. The conventional notion is that the low ADC value of TNBC is associated with abnormal proliferation of stromal cells. High cell density leads to a decrease in the extracellular space volume fraction, thereby exacerbating the restricted diffusion of water molecules. However, our study found that the ADC value of the TNBC group was higher than that of the non-TNBC group. This may be because the rapid proliferation of TNBC tumor cells exceeds neovascularization, causing local tissue hypoxia and microscopic necrosis, and during the necrosis process, cell membrane rupture accelerates the diffusion of water molecules [30]. In our group, the "necrosis effect" outweighed the "cellularity effect", leading to an increase in the ADC value. In addition, the high vascular permeability and loose endothelial junctions of TNBC promote the rapid extravasation of intravascular fluid into the extracellular space, facilitating diffusion. Therefore, the elevated ADC value in TNBC reflects the abnormal proliferation and necrosis of the tumor, rather than low cellularity [31].

The clinical application of mean ADC values is limited by scanner inhomogeneity, *b*-value selection, and physiological variability [11, 32]. To reduce the interference of confounding factors, this study used rADC values for analysis [13, 14]. The results showed that the performance of rADC1 (normalized to the ipsilateral pectoralis major muscle; AUC = 0.669) was superior to the mean ADC and rADC2 (normalized to the contralateral gland). This is consistent with the characteristic that the ADC value of the pectoralis major muscle is less affected by breast type, pathological status, and hormone levels [13]. In contrast, the contralateral gland may change with hormone fluctuations during the menstrual cycle, and is related to factors such as anatomical heterogeneity (e.g., asymmetry in gland density and fat content), reducing the reliability and diagnostic performance of rADC2 [33].

The high OR associated with rADC1 reflects a statistical artifact called "quasi-complete separation". Within a certain threshold range, the data exhibit a minimal overlap area, leading to a mathematically amplified OR. Although the confidence interval is large, Bootstrap validation confirmed that its diagnostic performance remains statistically significant.

Although rADC is not a novel parameter, we are more concerned with its clinical utility. Although radiomics or deep learning methods have higher accuracy [34, 35], they are opaque "black boxes", that require specialized software and complex biological explanations, which limits their clinical application. In contrast, rADC is easier to obtain, can be measured on a workstation, and allows for biological interpretation. Compared with complex algorithms, rADC provides quantifiable indicators that are more suitable for clinical practice.

Because the diagnostic specificity of a single parameter is limited, we established a multiparametric model including rADC1, peritumoral edema, and multifocality. This model had good discriminative performance in the validation set (AUC = 0.772), which was superior to that of other single-parameter models. Morphological features such as peritumoral edema indicate the aggressiveness and spread of the tumor, while rADC1 provides a quantitative and standardized evaluation indicator for the intratumoral microenvironment.

We know that the AUC of the combined model is 0.772, which only represents moderate discriminatory ability. Because TNBC often overlaps with benign lesions (especially masses with smooth margins) in imaging manifestations, differential diagnosis on imaging is relatively difficult [36]. Under such difficulties, our combined model still shows balanced predictive performance and has good clinical practical value. The sensitivity of the combined model is 67.19%, the PPV is 55.8%, and the NPV is as high as 84.6%. In contrast, although using rADC2 alone has high sensitivity, its specificity is low (37.58%), which causes higher false positives. Therefore, the multivariate combined method significantly improves the reliability of diagnosing TNBC. In terms of clinical utility, although the sensitivity of the model is moderate, the high NPV enables clinicians to confidently exclude non-TNBC subtypes and focus their energy on the evaluation of suspicious cases. In addition, DCA further confirmed the clinical utility of the model; compared with "treat-all" or "treat-none" strategies, the model shows a higher net benefit across a wide range of threshold probabilities. The multiparametric model can help clinicians effectively identify TNBC patients preoperatively, provide a basis for formulating personalized neoadjuvant treatment or surgical plans, thereby optimizing treatment strategies and ultimately improving patient prognosis.

Limitations

This study has several limitations. First, as a single-center retrospective study, selection bias may exist. Although we used 1,000 Bootstrap iteration resampling to reduce errors, multicenter and large-sample studies are needed in the future. Second, this study excluded NME lesions. This narrowed the application scope of the study. However, the reason for doing this is that NME often overlaps with normal glandular tissue and is prone to producing partial volume effects, thereby reducing the accuracy of ADC. Therefore, our current model is only used for mass-like tumors. Third, regarding the limitation of ROI measurement, our study only used the two-dimensional region of interest at the largest slice of the tumor, rather than the three-dimensional volume segmentation of the tumor. This may ignore the spatial heterogeneity within the tumor. Fourth, there is a lack of molecular genetic data. This study did not collect the BRCA mutation status of the patients. Future research is needed to further study the radiogenomic association between MRI imaging features and specific TNBC genotypes to fill this gap.

Conclusion

In summary, TNBC and non-TNBC have significant differences in MRI morphology, hemodynamics, and diffusion coefficients. The multiparametric combined model for predicting TNBC, constructed by combining multifocality, peritumoral edema, and rADC1, has good discrimination and calibration, and has clinical utility. This model provides noninvasive evidence for accurately identifying TNBC, and provides an important imaging reference basis for the clinical formulation of individualized diagnosis and treatment plans.

Acknowledgements

This work was supported by the Undergraduate Innovation Training Program Project of Soochow University (Grant No. 2025C179).

Disclosure of conflict of interest

None.

Address correspondence to: Yue Teng and Xinxing Ma, Department of Radiology, The First Affiliated Hospital of Soochow University, No. 899 Pinghai Road, Suzhou 215006, Jiangsu, China. Tel: +86-13771767132; E-mail: tengyue@suda.edu.cn (YT); Tel: +86-15962145313; E-mail: xinxingma@suda.edu.cn (XXM)

References

[1] Sung H, Ferlay J, Siegel RL, Laversanne M, Soerjomataram I, Jemal A and Bray F. Global can-

cer statistics 2020: GLOBOCAN estimates of incidence and mortality worldwide for 36 cancers in 185 countries. CA Cancer J Clin 2021; 71: 209-249.

[2] Yau C, Osdoit M, van der Noordaa M, Shad S, Wei J, de Croze D, Hamy AS, Laé M, Reyal F, Sonke GS, Steenbruggen TG, van Seijen M, Wesseling J, Martín M, Del Monte-Millán M and López-Tarruella S; I-SPY 2 Trial Consortium, Boughey JC, Goetz MP, Hoskin T, Gould R, Valero V, Edge SB, Abraham JE, Bartlett JMS, Caldas C, Dunn J, Earl H, Hayward L, Hiller L, Provenzano E, Sammut SJ, Thomas JS, Cameron D, Graham A, Hall P, Mackintosh L, Fan F, Godwin AK, Schwensen K, Sharma P, DeMichele AM, Cole K, Pusztai L, Kim MO, van't Veer LJ, Esserman LJ and Symmans WF. Residual cancer burden after neoadjuvant chemotherapy and long-term survival outcomes in breast cancer: a multicentre pooled analysis of 5161 patients. Lancet Oncol 2022; 23: 149-160.

[3] Derakhshan F and Reis-Filho JS. Pathogenesis of triple-negative breast cancer. Annu Rev Pathol 2022; 17: 181-204.

[4] Bianchini G, De Angelis C, Licata L and Gianni L. Treatment landscape of triple-negative breast cancer - expanded options, evolving needs. Nat Rev Clin Oncol 2022; 19: 91-113.

[5] Lima M, Honda M, Sigmund EE, Ohno Kishimoto A, Kataoka M and Togashi K. Diffusion MRI of the breast: current status and future directions. J Magn Reson Imaging 2020; 52: 70-90.

[6] Meyer HJ, Wienke A and Surov A. Diffusion-weighted imaging of different breast cancer molecular subtypes: a systematic review and meta-analysis. Breast Care (Basel) 2022; 17: 47-54.

[7] Chen H, Li W, Wan C and Zhang J. Correlation of dynamic contrast-enhanced MRI and diffusion-weighted MR imaging with prognostic factors and subtypes of breast cancers. Front Oncol 2022; 12: 942943.

[8] Bickel H, Clauser P, Pinker K, Helbich T, Biondic I, Brkljacic B, Dietzel M, Ivanac G, Krug B, Moschetta M, Neuhaus V, Preidler K and Baltzer P. Introduction of a breast apparent diffusion coefficient category system (ADC-B) derived from a large multicenter MRI database. Eur Radiol 2023; 33: 5400-5410.

[9] Lin CX, Tian Y, Li JM, Liao ST, Liu YT, Zhan RG, Du ZL and Yu XR. Diagnostic value of multiple b-value diffusion-weighted imaging in discriminating the malignant from benign breast lesions. BMC Med Imaging 2023; 23: 10.

[10] Dkhar W, Kadavigere R, Ravichandran S, Pradhan A, Sukumar S and Barnes Abraham N. Hormonal influences on ADC values in breast tissues: a scoping review of DWI in pre- and post-menopausal women. F1000Res 2025; 13: 857.

[11] Baltzer P, Mann RM, Iima M, Sigmund EE, Clauser P, Gilbert FJ, Martincich L, Partridge SC, Patterson A, Pinker K, Thibault F, Camps-Herrero J and Le Bihan D; EUSOBI international Breast Diffusion-Weighted Imaging working group. Diffusion-weighted imaging of the breast-a consensus and mission statement from the EUSOBI International Breast Diffusion-Weighted Imaging working group. Eur Radiol 2020; 30: 1436-1450.

[12] Newitt DC, Zhang Z, Gibbs JE, Partridge SC, Chenevert TL, Rosen MA, Bolan PJ, Marques HS, Aliu S, Li W, Cimino L, Joe BN, Umphrey H, Ojeda-Fournier H, Dogan B, Oh K, Abe H, Drukteinis J, Esserman LJ and Hylton NM; ACRIN Trial Team and I-SPY 2 TRIAL Investigators. Test-retest repeatability and reproducibility of ADC measures by breast DWI: results from the ACRIN 6698 trial. J Magn Reson Imaging 2019; 49: 1617-1628.

[13] Tang W, Chen L, Jin Z, Liang Y, Zuo W, Wei X, Guo Y, Kong Q and Jiang X. The diagnostic dilemma with the plateau pattern of the time-intensity curve: can the relative apparent diffusion coefficient (rADC) optimise the ADC parameter for differentiating breast lesions? Clin Radiol 2021; 76: 688-695.

[14] Weng C, Yang Y, Yang L, Hu C, Ma X and Li G. Evaluations of the diagnostic performance of ZOOMit diffusion-weighted imaging and conventional diffusion-weighted imaging for breast lesions. Quant Imaging Med Surg 2023; 13: 8478-8488.

[15] Li X, Sun K, Chai W, Zhu H and Yan F. Role of breast MRI in predicting histologic upgrade risks in high-risk breast lesions: a review. Eur J Radiol 2021; 142: 109855.

[16] Nadrljanski MM and Milosevic ZC. Relative apparent diffusion coefficient (rADC) in breast lesions of uncertain malignant potential (B3 lesions) and pathologically proven breast carcinoma (B5 lesions) following breast biopsy. Eur J Radiol 2020; 124: 108854.

[17] Allison KH, Hammond MEH, Dowsett M, McKernin SE, Carey LA, Fitzgibbons PL, Hayes DF, Lakhani SR, Chavez-MacGregor M, Perlmutter J, Perou CM, Regan MM, Rimm DL, Symmans WF, Torlakovic EE, Varella L, Viale G, Weisberg TF, McShane LM and Wolff AC. Estrogen and progesterone receptor testing in breast cancer: ASCO/CAP guideline update. J Clin Oncol 2020; 38: 1346-1366.

[18] Wolff AC, Somerfield MR, Dowsett M, Hammond MEH, Hayes DF, McShane LM, Saphner TJ, Spears PA and Allison KH. Human epidermal growth factor receptor 2 testing in breast

cancer: ASCO-college of American pathologists guideline update. J Clin Oncol 2023; 41: 3867-3872.
[19] Pont M, Marqués M and Sorolla A. Latest therapeutical approaches for triple-negative breast cancer: from preclinical to clinical research. Int J Mol Sci 2024; 25: 13518.
[20] Rugengamanzi E, Dharsee N, Lugina EL, Kashabano JJ, Murenzi G, Paciorek A, Malangwa G, Banzi M, Makupa G, Nnko G, Mwakipunda L and Lee AY. Comparison of clinicopathological features and survival in triple-negative and non-triple-negative breast cancer patients in Tanzania. Oncologist 2025; 30: oyaf345.
[21] So JY, Ohm J, Lipkowitz S and Yang L. Triple negative breast cancer (TNBC): non-genetic tumor heterogeneity and immune microenvironment: emerging treatment options. Pharmacol Ther 2022; 237: 108253.
[22] Moffa G, Galati F, Collalunga E, Rizzo V, Kripa E, D'Amati G and Pediconi F. Can MRI Biomarkers predict triple-negative breast cancer? Diagnostics (Basel) 2020; 10: 1090.
[23] Valluri AR, Carter GJ, Robrahn I and Berg WA. Triple-negative breast cancer: radiologic-pathologic correlation. J Breast Imaging 2025; 7: 331-344.
[24] Cai Y, Li Y, Wang W, Zhou Y, Wang J, Zhang L and Lu H. A machine-learning model for the prediction of triple-negative breast cancer based on multiparameter MRI. Breast Cancer (Dove Med Press) 2025; 17: 611-625.
[25] Adrada BE, Moseley TW, Kapoor MM, Scoggins ME, Patel MM, Perez F, Nia ES, Khazai L, Arribas E, Rauch GM and Guirguis MS. Triple-negative breast cancer: histopathologic features, genomics, and treatment. Radiographics 2023; 43: e230034.
[26] Panzironi G, Moffa G, Galati F, Marzocca F, Rizzo V and Pediconi F. Peritumoral edema as a biomarker of the aggressiveness of breast cancer: results of a retrospective study on a 3 T scanner. Breast Cancer Res Treat 2020; 181: 53-60.
[27] Chen H, Min Y, Xiang K, Chen J and Yin G. DCE-MRI performance in triple negative breast cancers: comparison with non-triple negative breast cancers. Curr Med Imaging 2022; 18: 970-976.
[28] Matsuda M, Tsuda T, Ebihara R, Toshimori W, Okada K, Takeda S, Okumura A, Shiraishi Y, Suekuni H, Kamei Y, Kurata M, Kitazawa R, Mochizuki T and Kido T. Triple-negative breast cancer on contrast-enhanced MRI and synthetic MRI: a comparison with non-triple-negative breast carcinoma. Eur J Radiol 2021; 142: 109838.
[29] Ohashi A, Kataoka M, Iima M, Honda M, Ota R, Urushibata Y, Dominik Nickel M, Toi M, Zackrisson S and Nakamoto Y. A multiparametric approach to predict triple-negative breast cancer including parameters derived from ultrafast dynamic contrast-enhanced MRI. Eur Radiol 2023; 33: 8132-8141.
[30] Yetkin Dİ, Akpınar MG, Durhan G and Demirkazik FB. Comparison of clinical and magnetic resonance imaging findings of triple-negative breast cancer with non-triple-negative tumours. Pol J Radiol 2021; 86: e269-e276.
[31] Santucci D, Faiella E, Calabrese A, Beomonte Zobel B, Ascione A, Cerbelli B, Iannello G, Soda P and de Felice C. On the additional information provided by 3T-MRI ADC in predicting tumor cellularity and microscopic behavior. Cancers (Basel) 2021; 13: 5167.
[32] Kim YS, Yun B, Chu AJ, Lee SH, Shin HJ, Kim SM, Jang M, Shin SU and Moon WK. Background breast parenchymal signal during menstrual cycle on diffusion-weighted MRI: a prospective study in healthy premenopausal women. Korean J Radiol 2024; 25: 511-517.
[33] Lim Y, Ko ES, Han BK, Ko EY, Choi JS, Lee JE and Lee SK. Background parenchymal enhancement on breast MRI: association with recurrence-free survival in patients with newly diagnosed invasive breast cancer. Breast Cancer Res Treat 2017; 163: 573-586.
[34] Ma M, Gan L, Jiang Y, Qin N, Li C, Zhang Y and Wang X. Radiomics analysis based on automatic image segmentation of DCE-MRI for predicting triple-negative and nontriple-negative breast cancer. Comput Math Methods Med 2021; 2021: 2140465.
[35] Qi YJ, Su GH, You C, Zhang X, Xiao Y, Jiang YZ and Shao ZM. Radiomics in breast cancer: current advances and future directions. Cell Rep Med 2024; 5: 101719.
[36] Schopp JG, Polat DS, Arjmandi F, Hayes JC, Ahn RW, Sullivan K, Sahoo S and Porembka JH. Imaging challenges in diagnosing triple-negative breast cancer. Radiographics 2023; 43: e230027.